

Microstructure and velocity fluctuations in sheared suspensions

By GERMAN DRAZER¹, JOEL KOPLIK¹,
BORIS KHUSID² AND ANDREAS ACRIVOS¹

¹The Levich Institute, T-1M, The City College of the City University
of New York, New York, NY 10031, USA

²Department of Mechanical Engineering, New Jersey Institute of Technology,
University Heights, Newark, NJ 07102, USA

(Received 21 July 2003 and in revised form 12 March 2004)

The velocity fluctuations present in macroscopically homogeneous suspensions of neutrally buoyant non-Brownian spheres undergoing simple shear flow, and their dependence on the microstructure developed by the suspensions, are investigated in the limit of vanishingly small Reynolds numbers using Stokesian dynamics simulations. We show that, in the dilute limit, the standard deviation of the velocity fluctuations (the so-called suspension temperature) is proportional to the volume fraction, in both the transverse and the flow directions, and that a theoretical prediction, which considers only the hydrodynamic interactions between isolated pairs of spheres, is in good agreement with the numerical results at low concentrations. We also simulate the velocity fluctuations that would result from a random hard-sphere distribution of spheres in simple shear flow, and thereby investigate the effects of the microstructure on the velocity fluctuations. Analogous results are discussed for the fluctuations in the angular velocity of the suspended spheres. In addition, we present the probability density functions for all the linear and angular velocity components, and for three different concentrations, showing a transition from a Gaussian to an exponential and finally to a stretched exponential functional form as the volume fraction is decreased.

The simulations include a non-hydrodynamic repulsive force between the spheres which, although extremely short range, leads to the development of fore–aft asymmetric distributions for large enough volume fractions, if the range of that force is kept unchanged. On the other hand, we show that, although the pair distribution function recovers its fore–aft symmetry in dilute suspensions, it remains anisotropic and that this anisotropy can be accurately predicted theoretically from the two-sphere solution by assuming the complete absence of any permanent doublets of spheres.

We also present a simple correction to the analysis of laser-Doppler velocimetry measurements, which substantially improves the interpretation of these measurements at low volume fractions even though it involves only the angular velocity of a single sphere in the vorticity direction.

Finally, in an Appendix, we show that, in the dilute limit, the whole velocity autocorrelation function can be predicted using again only two-particle encounters.

1. Introduction

The problem of determining the velocity fluctuations in suspensions of non-Brownian solid spheres in Stokes flows is one of long-standing difficulty owing to the

underlying long-range many-body hydrodynamic interactions between the suspended particles. Even an apparently very simple case, that of determining the dependence on the shear rate of the velocity fluctuations in simple shear flows, remains a matter of some controversy (Shapley, Armstrong & Brown 2002). What is clear is that, although the suspension might be homogeneous at macroscopic scales, the continuous rearrangements in the suspension microstructure and the corresponding hydrodynamic interactions between particles lead to fluctuations in the particle velocities about their mean values, in both the transverse and the flow directions.

In our previous work (Drazer *et al.* 2002, hereinafter referred to as paper 1), we showed that the dynamics of sheared suspensions is chaotic and offered evidence that the chaotic motion is responsible for the loss of memory in the evolution of the system. This loss of memory, coupled with the fluctuations in the velocity of the spheres, ultimately leads to the phenomenon of shear-induced particle diffusion.

The variance, or the standard deviation (STD), of the velocity fluctuations is the simplest measure of the magnitude of such fluctuations and is sometimes referred to as the suspension *temperature*, which in the case of an anisotropic motion of the suspended spheres would actually be a tensor (covariance matrix). The notion of suspension temperature was introduced by Nott & Brady (1994) in a continuum model aimed at calculating steady-state velocity and concentration profiles in flows of concentrated suspensions. In fact, velocity fluctuations lead to the migration and diffusion of particles in shear flows, phenomena that occur in a wide variety of natural as well as engineering problems, ranging from the dispersion and migration of red blood cells (Bishop *et al.* 2002) to the food industry (Cullen *et al.* 2000; Gotz, Zick & Kreibich 2003), hence it is important to determine their properties. In particular, we are interested in the dependence of the velocity fluctuations on the concentration and microstructure of the suspension. Unfortunately, and in contrast to the well-studied sedimentation problem, velocity fluctuations in sheared suspensions have received little attention thus far. In recent experiments, Averbakh *et al.* (1997), Shauly *et al.* (1997), Lyon & Leal (1998) and Shapley *et al.* (2002) used laser-Doppler velocimetry (LDV) to measure the velocity fluctuations in concentrated suspensions of monodisperse spheres. Averbakh *et al.* (1997) and Shauly *et al.* (1997) measured such velocity fluctuations in rectangular ducts and found that the STDs, both along and transverse to the flow, depend linearly on the shear rate (or on the maximum velocity inside the rectangular channel), as expected in the Stokes limit[†]. Lyon & Leal (1998) measured the time-averaged local STD in the direction of the flow, for concentrated suspensions flowing in a two-dimensional rectangular channel, and also found a linear dependence on the volumetric flow rate. Shapley *et al.* (2002) presented the first detailed measurements of the velocity fluctuations in both the transverse and the flow directions, as well as of the dependence of the suspension temperature on the volume fraction and shear rate, for suspensions undergoing simple shear flow in a Couette device. Their results stress the difficulties encountered in such measurements and the discrepancy among different experimental results. They found a highly anisotropic temperature tensor, with the magnitude of the fluctuations, in both the transverse components of the velocity being smaller than that in the direction of the bulk flow. Shapley *et al.* (2002) also found that the temperature was not a monotonically increasing function of the volume fraction, as is usually expected, but that it showed

[†] Let us note that in these experiments, the main contribution to the measured STDs were not actual fluctuations but migration and angular velocities of the suspended particles, as noted by the authors.

a different behaviour for each of its components. Specifically, the component of the temperature in the direction of flow was found to decrease with concentration, that in the direction of the gradient stayed constant, while that in the vorticity direction initially increased in magnitude with increasing concentrations and then decreased for concentrations larger than 40%. Finally, and most surprisingly, Shapley *et al.* (2002) found that, whereas the fluctuations in the direction of the flow increased linearly with shear rate (as expected for any flow in the Stokes regime), the STD in the vorticity direction increased nonlinearly, while that in the gradient direction slightly decreased with shear rate.

In terms of the suspension spatial structure, although a larger body of experimental information exists concerning the microscopic structure developed by suspensions of monodisperse non-Brownian spheres undergoing linear shear flow, no measurements of how the velocity fluctuations are affected by the suspension microstructure appear to have been conducted thus far. Recall that the experimental work of Gadala-Maria & Acrivos (1980) provided, for the first time, clear evidence that concentrated suspensions of monodisperse non-Brownian spheres develop an anisotropic structure when sheared. They showed that, when the direction of shear was reversed, the shear stress measured in a parallel plate device underwent a transient response not present when the shearing was started again in the same direction, and thereby concluded that the underlying structure was not only anisotropic but asymmetric under reversal of the flow direction, i.e. fore–aft asymmetric. Their oscillatory experiments showed similar results, in that the measured dynamic viscosity μ' , although independent of the frequency of oscillation at low frequencies, was consistently smaller than the shear viscosity μ of the suspension, stressing again the presence of a microscopic structure induced by the shear. In recent experiments, Kolli, Pollauf & Gadala-Maria (2002) used a parallel ring geometry that allowed them to measure the normal stress response to shear reversal in concentrated suspensions, in addition to measuring the shear stress behaviour, and found a transient response in both the normal and the shear stresses when the direction of shear was reversed. Moreover, the absolute value of both the normal and the shear stresses changed at the very instant of flow reversal, which means that the fore–aft asymmetry in the microstructure alone is not enough to explain the observed response in the stress upon shear reversal, but that non-hydrodynamic forces must also have been acting on the system, either in the form of repulsion forces or of rough contacts between spheres. Even more complicated shear stress responses, including shear-induced ordering, have been recently reported at large concentrations ($\phi > 50\%$), probably corresponding to a regime in which non-hydrodynamic interactions dominate the behaviour of the system (Voltz *et al.* 2002). The first direct observations of the microscopic structure developed by dilute suspensions ($\phi = 1\%–5\%$) undergoing shear were presented by Husband & Gadala-Maria (1987), who measured in a Couette device the relative distribution of the sphere centres in the plane of shear, and then by averaging over many realizations, found an anisotropic but fore–aft symmetric distribution of close particles. The anisotropy was attributed to the presence of pairs of spheres rotating around each other forming permanent doublets. On the other hand, in similar experiments, Parsi & Gadala-Maria (1987) showed that concentrated suspensions ($\phi = 40\%–50\%$) do exhibit fore–aft asymmetry, with a larger probability of finding pairs of spheres oriented on the approaching side of the reference particle, and attributed this asymmetric distribution to either the intrinsic roughness of the spheres or the presence of a non-hydrodynamic repulsive force between particles. Rampall, Smart & Leighton (1997) used a substantially improved flow-visualization technique

to measure the pair distribution function of dilute suspensions ($\phi = 5\% - 15\%$) undergoing simple shear flow in a shear tank apparatus, and showed that, contrary to the results of Husband & Gadala-Maria (1987), there is a depletion of permanent doublets moving in the region of closed streamlines, and that even for concentrations as small as 5%, the distribution is fore–aft asymmetric. Using the surface roughness model of da Cunha & Hinch (1996), and assuming that no particles formed permanent doublets, Rampall *et al.* (1997) were able to reproduce the qualitative trends in the pair distribution function, but the predicted depletion of spheres in the regions aligned with the flow was much larger than that observed.

In view of the contradictory results outlined before, it is clear that numerical simulations, specifically Stokesian dynamics which are well suited to the study of low-Reynolds number flows of suspensions (Brady 2001), offer an important complement to experiments, in that they can provide detailed microscopic information that is not accessible via currently available experimental techniques. In their original work describing their Stokesian dynamics method, Bossis & Brady (1984) showed that the pair distribution function of unbounded suspensions undergoing simple shear flow had an angular dependence, with the microstructure being no longer fore–aft symmetric, and that very few particles were oriented in the receding side of the reference sphere. Following this pioneering work, several studies investigated the microstructure developed by both Brownian and non-Brownian suspensions in shear flow. Sierou & Brady (2002) showed that, in a suspension of non-Brownian particles, nearly touching spheres are distributed anisotropically, with most of the pairs oriented along the compressional axis. Morris & Katyal (2002) presented similar results for the microstructure of Brownian suspensions at large shear rates. In paper 1, we also showed such a break in the fore–aft symmetry in the presence of large non-hydrodynamic forces acting between the spheres, but, for sufficiently small repulsion forces, we found that, although anisotropic, the pair distribution function becomes fore–aft symmetric, as expected for purely hydrodynamic interactions. To our knowledge, however, as yet no systematic numerical investigation has been made of the velocity fluctuations in sheared suspensions and their dependence on the underlying microstructure of the suspension.

It is the purpose of this paper to investigate the velocity fluctuations present in a macroscopically homogeneous unbounded suspension of neutrally buoyant non-Brownian spheres subject to a simple shear flow in the limit of vanishingly small Reynolds numbers using Stokesian dynamics, as well as their dependence on the suspension microstructure generated by the shear. First, we shall focus on the anisotropic, but fore–aft symmetric, pair distribution function of spheres in close proximity observed in dilute suspensions, and show how it can be accurately described assuming the absence of permanent doublets of spheres, as first suggested by Rampall *et al.* (1997). We shall also point out that, although the use of a non-hydrodynamic interparticle force of extremely short range will yield symmetric distributions, as was reported in paper 1, the suspensions develop a fore–aft asymmetry for large enough volume fractions if the range of that force is kept unchanged. Then, we shall show that the pair distribution function $g_{BG}(r)$ obtained by Batchelor & Green (1972*b*) in the dilute limit (by *dilute limit* we refer to results obtained by neglecting hydrodynamic interactions between three or more spheres, which therefore could be expected to apply only in the limit of low volume fractions), accurately describes the microstructure in sheared suspensions, in particular, the divergence of the probability density of finding pairs of spheres nearly touching one another, even though it does not account for the observed depletion of closed pairs. Then, by making use of this pair distribution

function $g_{BG}(r)$, we shall compute all the temperature components in the dilute limit by numerically integrating the expressions given by Batchelor & Green (1972a) for the particle velocities of two freely suspended spheres interacting only through hydrodynamic forces in the presence of a simple shear flow, following which we shall compare the results with those obtained from the numerical simulations. Some general properties of the temperature tensor valid for isotropic pair distribution functions will also be discussed. The velocity fluctuations at larger concentrations show the effect of the anisotropic structure developed by the flow in that some of the low-concentration symmetries of the temperature tensor are lost. We also simulate the velocity fluctuations that would result from a random hard-sphere spatial distribution of particles in a simple shear flow, and thereby are able to further investigate the effects of the microstructure, both its angular and radial dependence, on the temperature tensor. In addition, the numerical simulations provide a full picture of the velocity fluctuations and therefore allow us to compute the probability density functions for all the linear and angular velocity components at three different concentrations, which show a transition from a Gaussian to an exponential and finally to a stretched exponential form as the volume fraction is decreased. Finally, we shall propose a simple correction to the data reduction analysis of velocity measurements in LDV experiments which substantially improves the interpretation of such measurements at low volume fractions even though it involves only the angular velocity of a single sphere in the vorticity direction.

2. Simulation method: Stokesian dynamics

We investigate the behaviour of suspensions of non-Brownian particles subject to simple shear using the method of Stokesian dynamics. A detailed description of the method is given in Brady & Bossis (1988), and the specifics of our simulations have been discussed in paper 1, hence only a brief discussion is presented here. The method accounts for the hydrodynamic forces between solid spheres undergoing simple shear, characterized by a shear rate $\dot{\gamma}$, in the limit of zero Reynolds number. In order to simulate the behaviour of infinite suspensions, periodic boundary conditions in all directions are imposed. The simulated cubic cell contains a fixed number of spheres N , related to the volume fraction ϕ by $\phi = (4\pi a^3/3)N/V$, where V is the volume of the cell. Interactions between particles more than a cell apart are included using the Ewald method. A typical simulation consisted of $N = 64$ particles sheared over a period of time $t \sim 100\dot{\gamma}^{-1}$, and all measurements to be reported in this work are for strains $\dot{\gamma}t$ in excess of 50, when the system has reached its steady or fully developed state. The motion of the particles was integrated using a constant time step $\Delta t = 10^{-3}\dot{\gamma}^{-1}$. The results are averaged over $N_c \sim 100$ different initial configurations, with each initial configuration corresponding to a random distribution of non-overlapping spheres in the simulation cell, using the random-phase average method proposed by Marchioro & Acrivos (2001). In what follows, we shall express all the variables in dimensionless units, using the radius of the spheres a as the characteristic length and $\dot{\gamma}^{-1}$ as the characteristic time.

In a suspension of monodisperse spheres undergoing simple shear, the separation between spheres may become exceedingly small during two-particle collisions (less than 10^{-4} of their radius), and the effects of surface roughness or small Brownian displacements cannot be neglected. Usually, a short-range repulsive force is introduced between the spheres to qualitatively model the effect of these non-hydrodynamic interactions, with the numerical advantage of preventing any overlaps during close

encounters between particles. As in paper 1, we used the following standard expression for the repulsive interparticle force,

$$\mathbf{F}_{\alpha\beta} = \frac{F_0}{r_c} \frac{e^{-\epsilon/r_c}}{1 - e^{-\epsilon/r_c}} \mathbf{e}_{\alpha\beta}, \quad (2.1)$$

where $6\pi\mu a^2\dot{\gamma}\mathbf{F}_{\alpha\beta}$, with μ being the viscosity of the suspending liquid, is the force exerted on sphere α by sphere β , F_0 is a dimensionless coefficient reflecting the magnitude of this force, r_c is the characteristic range of the force, ϵ is the distance of closest approach between the surfaces of the two spheres divided by a , and $\mathbf{e}_{\alpha\beta}$ is the unit vector connecting their centres pointing from β to α .

The effect of the characteristic range of the interparticle force r_c on the microscopic structure of the suspension was discussed in paper 1. First, we showed that the minimum separation reached by colliding spheres, and therefore the first peak in the pair distribution function, is strongly affected by the range of the interparticle force in that, as r_c increases, the minimum separation between neighbouring particles also increases. Then, we showed that, in general, the presence of a repulsive force breaks the fore-aft symmetry of the particle trajectories in a simple shear flow. However, we also showed that the symmetry is recovered, for small enough values of the force range, $r_c \sim 10^{-4}$, at least in the sense that no asymmetry was observed in the angular dependence of the numerically computed pair distribution function. In this work, we use this small range for the interparticle force, $r_c \sim 10^{-4}$, together with $F_0 = 1$.

3. Microscopic structure induced by the shear

The investigation of the microscopic structure developed by suspensions undergoing shear flow followed the pioneering work by Batchelor & Green (1972*b*), who considered the probability $P(\mathbf{r}|\mathbf{r}_0 = 0)$ of finding a sphere with its centre at \mathbf{r} , given that there is a sphere with its centre at $\mathbf{r}_0 = 0$, in the dilute limit when $P(\mathbf{r}|\mathbf{r}_0 = 0) = \phi p(\mathbf{r})(3/4\pi)$. Recall that, even a random hard-sphere distribution leads to correlations in the position of any two particles owing to excluded volume effects, and typically displays a liquid-like microstructure at high volume fractions. However, in addition to these excluded volume effects, hydrodynamic interactions between spheres lead to surprising results. By solving the equations for the motion of two particles subject to a simple shear flow, Batchelor & Green (1972*a*) showed that $p(\mathbf{r})/g(r)$, with $g(r)$ given by (3.1) below, is constant for a material point in \mathbf{r} -space. Then, by assuming that the positions of two particles which originate from infinity along an open trajectory are not correlated, Batchelor & Green (1972*a*) showed that the pair distribution function is an isotropic function of the distance between two spheres, i.e. $p(\mathbf{r}) = g(r)$, and that it diverges as $r \rightarrow 2$, which means that pairs of particles are substantially more likely to be found near contact in a sheared suspension than in a random hard-sphere distribution. In turn, this implies a high correlation in the position of the spheres that is not present in a random hard-sphere configuration. The expression for $g(\mathbf{r})$ derived by Batchelor & Green (1972*b*) is,

$$g_{BG}(r) = \frac{1}{1 - A(r)} \exp \left\{ \int_r^\infty \frac{3}{\xi} \frac{B(\xi) - A(\xi)}{1 - A(\xi)} d\xi \right\}, \quad (3.1)$$

where the mobility functions A and B are functions only of r . Here, we shall use the expressions for these functions given by da Cunha & Hinch (1996), who divided the interval $r > 2$ into three different regions: (a) the *lubrication* region $2 < r \leq 2.01$;

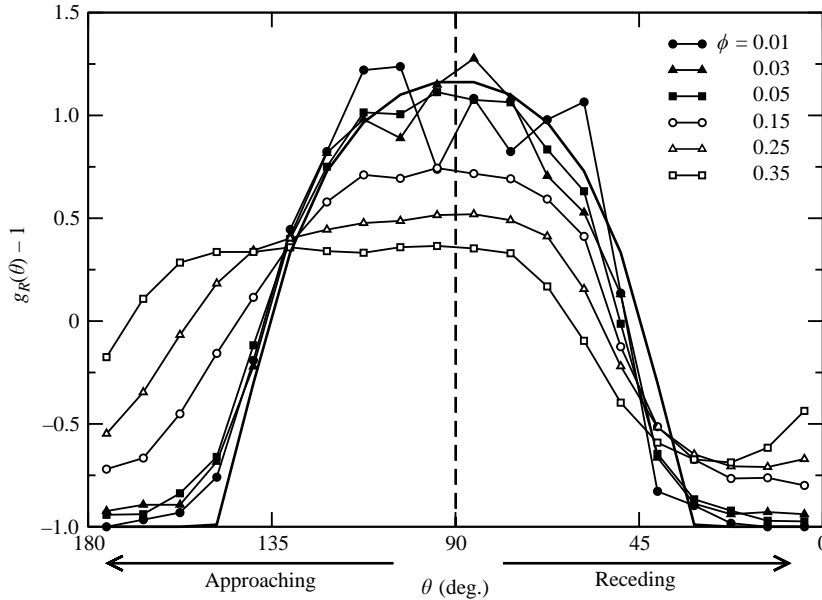


FIGURE 1. Normalized angular distribution function $g_R(\theta)$ for pairs of particles. The distance between the pairs lies in the range $2 < r < 2.01$ ($R = 2.01$). Different curves are for different volume fractions. All simulations were performed with $N = 64$, $N_c = 100$, $F_0 = 1$ and $r_c = 10^{-4}$. The solid line is obtained using the pair distribution function given in (3.1) for the region outside the closed streamlines and assuming that there is zero probability of finding a pair forming a permanent doublet.

(b) the *intermediate* region $2.01 < r \leq 2.5$; and (c) the *far-field* region $r > 2.5$ (see Appendix A for details).

To be precise, these results for the pair distribution function $g_{BG}(r)$, apply only to particles that are initially far from each other, and therefore spatially uncorrelated. However, in the limit of purely hydrodynamic interactions and very dilute suspensions (no three-particle interactions), there is a region of closed trajectories in \mathbf{r} -space, where pairs of particles remain correlated at all times forming permanent doublets (Batchelor & Green 1972a). In this case, the determination of the value of $p(\mathbf{r})/g(r)$ for particles forming permanent doublets would require the knowledge of the initial distribution of these particles. On the other hand, the presence of any non-hydrodynamic interaction, such as roughness or repulsion forces, or the existence of three-particle collisions, would generate a transfer of particles across the streamlines and therefore remove the need for specifying the initial distribution of spheres. Even so, to obtain the probability distribution would still require the full knowledge of the transfer process (the combination of three-particle collisions and non-hydrodynamic interactions), and the solution of the corresponding boundary-value problem.

This implies that the pair distribution function may actually be anisotropic simply because of the distribution of pairs forming permanent doublets in that, although the distribution of particles outside the region of closed streamlines does not have an angular structure in the dilute limit, as shown by Batchelor & Green (1972b), the distribution of particles in the region of closed streamlines, which in fact extends to $r \rightarrow \infty$, may actually render the complete pair distribution function anisotropic. In fact, in paper 1, we showed that, although for exceedingly short-range repulsion

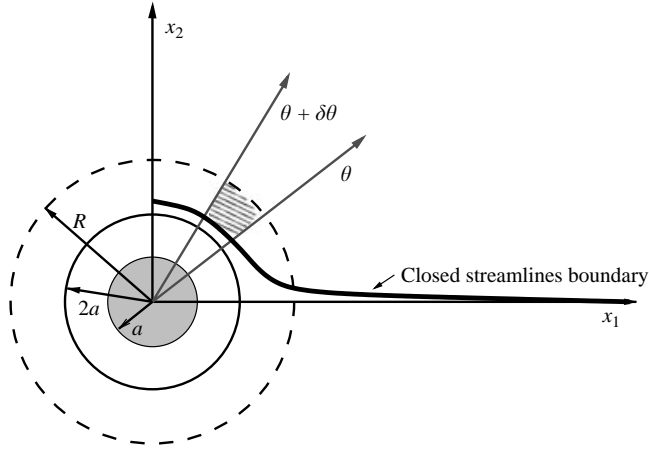


FIGURE 2. Schematic representation of the computation of $g_R(\theta)$ using the regions of open and closed streamlines for a pair of interacting spheres (Batchelor & Green 1972a). The solid line represents the intersection of the plane of shear $x_1 - x_2$ with the surface bounding the region of closed trajectories, which can be formed by rotating this curve about the x_2 -axis together with its mirror image obtained by reflection about the x_1 -axis. The grey circle of radius a represents the reference sphere and the circle of radius $2a$ encloses the excluded volume. Then, a particle with its centre located inside the sphere of radius R forms, with the reference sphere, a pair that is closer than R , and is included in $g_R(\theta)$. For a given angle θ , the distribution of pairs closer than R is calculated by integrating the pair distribution function given in (3.1) only in the shaded region, which corresponds to open trajectories, because the region of closed trajectories is considered to have a negligible effect owing to the depletion of permanent doublets.

forces, $r_c \sim 10^{-4}$, the pair distribution function for close particles recovered its expected fore-aft symmetry, it remained anisotropic. In figure 1, we present $g_R(\theta)$, the angular dependence of the pair distribution function of pairs closer than a certain distance R , as defined in paper 1, for different concentrations of the suspension (as mentioned in §2, all numerical results are for a range $r_c = 10^{-4}$ of the interparticle force, which is the smallest value of the force range simulated in paper 1). It can be seen that, even for this exceedingly short-range interparticle force, fore-aft symmetry is broken at large enough concentrations, and that the distributions show a larger number of pairs oriented on the approaching side of the reference sphere than on the receding side. Similar results have been reported for both Brownian (Morris & Katyal 2002) and non-Brownian (Sierou & Brady 2002) suspensions undergoing simple shear flow. More importantly, the angular distribution function seems to reach, in the dilute limit, an asymptotic distribution which is anisotropic and shows a depletion of pairs oriented close to the flow direction. This suggests a depletion of permanent doublets, which spend more time nearly aligned along the direction of the flow, and seems to indicate that, as speculated by Rampall *et al.* (1997), any mechanism forcing particles into the region of closed streamlines is small compared to the effect of the non-hydrodynamic forces which eliminate particles from this region, and ultimately leaves only a negligible number of pairs forming permanent doublets. In this case, the pair distribution function in the dilute limit should be the combination of $g_{BG}(r)$ for the region of open trajectories and a zero probability inside the region of closed streamlines. In figure 2, we show how we can then approximate the angular dependence of the pair distribution function of pairs closer than a certain distance

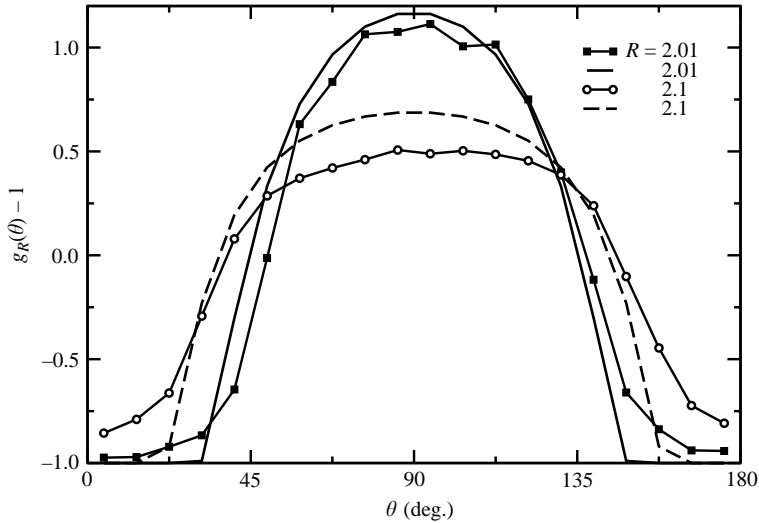


FIGURE 3. Angular distribution function $g_R(\theta)$ for pairs of particles corresponding to $R = 2.01$ and $R = 2.1$. The volume fraction is $\phi = 5\%$. The solid and dashed lines are obtained using the pair distribution function $g_{BG}(r)$ for the region of open trajectories and assuming zero probability inside the region of closed trajectories.

R , using the expression for the surface separating the regions of open and closed trajectories (Batchelor & Green 1972a),

$$x_2^2 = \exp \left\{ 2 \int_r^\infty \frac{A(\xi) - B(\xi) d\xi}{1 - A(\xi)} \frac{1}{\xi} \right\} \int_r^\infty \frac{B(\xi)}{1 - A(\xi)} \exp \left\{ -2 \int_\xi^\infty \frac{A(\zeta) - B(\zeta) d\zeta}{1 - A(\zeta)} \frac{1}{\zeta} \right\} \xi d\xi. \tag{3.2}$$

Clearly, the surface is axisymmetric with x_2 as the symmetry axis. (Here, and in what follows, the Cartesian axis 1 lies along the direction of the mean flow, 2 is perpendicular to 1 along the plane of shear, and 3 is the vorticity axis.)

In figure 1, we compare this approximation to the angular dependence of the pair distribution function of close pairs ($R = 2.01$) with the numerical results, and find a very good agreement for concentrations smaller than 5%. Moreover, in figure 3, we show that this approximation also accurately describes the anisotropy found for the pair distribution function of pairs when the range of separations is an order of magnitude larger, i.e. $R = 2.1$, thus validating the assumption of a complete depletion of pairs forming permanent doublets.

Finally, in figure 4, we present the radial dependence of the pair distribution function, i.e. the pair distribution function integrated over both spherical angles, as obtained from the numerical simulations at different particle concentrations. We also compare the numerical results with the pair distribution function given in (3.1), and find that, although $g_{BG}(r)$ does not account for the effect of the closed trajectories, in particular, the observed depletion of permanent doublets, it both follows the simulation results fairly accurately over a wide range of r and captures the substantial increase in the probability of finding pairs of particles near contact. Similar agreement between Stokesian dynamics simulations and $g_{BG}(r)$ has been reported for the case of Brownian spheres (Morris & Katyal 2002). On the other hand, $g_{BG}(r)$ seems to overestimate the asymptotic distribution in the dilute limit, and does not take into account the effects of the depletion of permanent doublets, which would

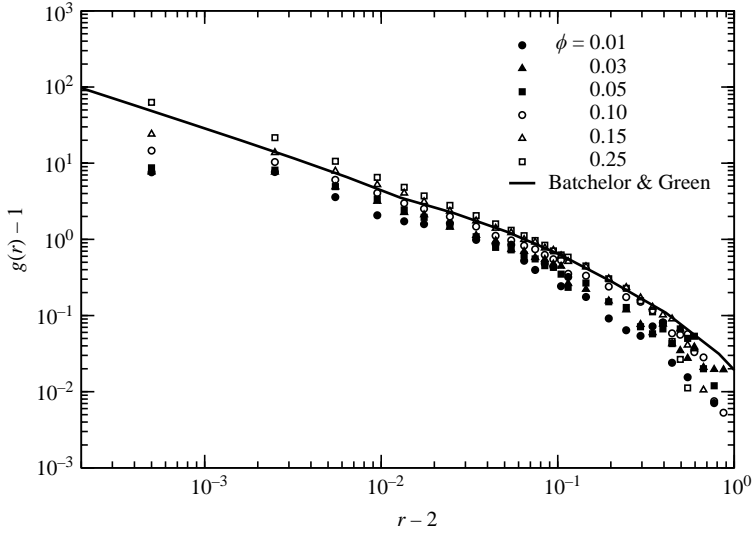


FIGURE 4. Pair distribution function integrated over all possible angular orientations. Different symbols correspond to the results obtained in numerical simulations for different volume fractions, $\phi = 0.25, 0.15, 0.10, 0.05$ and 0.03 . The pair distribution functions are constructed from a histogram of the distance between all pairs of particles, averaged over time and over different realizations (the smallest size of the bins in the histogram is $\Delta r = 0.0005$). The solid line corresponds to the pair distribution function given in (3.1).

ultimately lead to $g(r) = 0$ for r smaller than the minimum possible separation between approaching spheres in the region of open trajectories, $r_{\min} \sim 4 \times 10^{-5}$. However, for distances between the spheres that are not too small, $r \gtrsim 2.001$, (3.1) captures the divergent trend of $g(r)$ as $r \rightarrow 2$.

4. Velocity fluctuations

4.1. Analytical and numerical results

Following Batchelor's notation (Batchelor 1972) the temperature tensor (the covariance matrix of the velocity fluctuations (van Kampen 1987)) can be written as,

$$T_{ij} = \frac{1}{N!} \int d\mathcal{C}_{\mathcal{N}} \delta v_i(\mathbf{r}) \delta v_j(\mathbf{r}) P(\mathcal{C}_{\mathcal{N}}|\mathbf{r}), \quad (4.1)$$

where $\delta v_i(\mathbf{r})$ is the fluctuation in the velocity component v_i for a particle located at \mathbf{r} when the configuration of the surrounding spheres is given by $\mathcal{C}_{\mathcal{N}}$, with $P(\mathcal{C}_{\mathcal{N}}|\mathbf{r})$ being the probability of such an event. From its definition, it is clear that the temperature tensor is symmetric $T_{ij} = T_{ji}$. In addition, in simple shear flows, there exists an inversion symmetry in the vorticity direction, in that a given configuration and its counterpart in which x_3 is changed by $-x_3$ are equally probable, and therefore $T_{13} = T_{23} = 0$, for any volume fraction. We can simplify the temperature tensor even further by decomposing the simple shear flow into a solid-body rotating flow, which does not contribute to the velocity fluctuations irrespective of the concentration of particles, and a purely straining motion. The latter is symmetric in x_1 and x_2 and therefore, for any particular velocity fluctuation, say in the 1 direction, in a configuration $\mathcal{C}_{\mathcal{N}}$ of particles surrounding the reference sphere, the same fluctuation but in the 2 direction would be obtained by a configuration $\mathcal{C}'_{\mathcal{N}}$ in which all the

particle positions in $\mathcal{C}_{\mathcal{N}}$ are transformed according to $x_1 \leftrightarrow x_2$. Then, it clearly follows that $T_{11} = T_{22}$, depending only on whether the configurational probability density $P(\mathcal{C}_{\mathcal{N}}|\mathbf{r})$ has the same symmetry, i.e. it is invariant under the transformation $x_1 \leftrightarrow x_2$. Moreover, since a configuration $\mathcal{C}'_{\mathcal{N}}$ in which the particle positions in $\mathcal{C}_{\mathcal{N}}$ are transformed according to $x_1 \leftrightarrow -x_1$ would give the negative of the previous velocity fluctuation, and similarly for fluctuations in the 2 direction, it is clear that $T_{12} = 0$. Thus, the temperature tensor should be diagonal, as long as the probability density of particle configurations is invariant under those changes, i.e. as long as $P(\mathcal{C}_{\mathcal{N}}|\mathbf{r})$ remains invariant under the transformations $x_1 \leftrightarrow -x_1$ and $x_2 \leftrightarrow -x_2$.

In summary, for any concentration and a symmetry preserving configurational probability $P(\mathcal{C}_{\mathcal{N}}|\mathbf{r})$, we have that the off-diagonal terms of the temperature tensor are null and that the temperatures in the plane of shear are equal,

$$T_{ij} = 0 \quad (i \neq j), \quad (4.2)$$

$$T_{11} = T_{22}. \quad (4.3)$$

In the dilute limit, the fluctuations in the velocity come from two-particle interactions, and, from the far-field form of these interactions, it can be shown that any component of the temperature tensor, of the form $\delta v_i \delta v_j$, decays faster than $1/r^3$ and therefore, its average value can be directly computed by averaging the hydrodynamic interaction between a pair of spheres over all possible configurations,

$$T_{ij} = \int d\mathbf{r} \delta v_i \delta v_j (3\phi/4\pi) g(\mathbf{r}) = \phi \left[\frac{3}{4\pi} \int d\mathbf{r} \delta v_i \delta v_j g(\mathbf{r}) \right] = \phi t_{ij}, \quad (4.4)$$

which gives a linear dependence of the temperature components on the volume fraction, $T_{ij} = \phi t_{ij}$.

For two freely moving spheres in a simple shear flow, the velocity fluctuation of a sphere induced by a second centred at \mathbf{r} is given by (da Cunha & Hinch 1996):

$$\delta v_1 = \dot{x}_1 - x_2 = e x_1 - \frac{1}{2} B x_2, \quad (4.5)$$

$$\delta v_2 = e x_2 - \frac{1}{2} B x_1, \quad (4.6)$$

$$\delta v_3 = e x_3, \quad (4.7)$$

where $e = x_1 x_2 (B - A)/r^2$. Using these equations, it can be easily shown that, for a pair distribution function dependent only on r , not only is the temperature tensor diagonal, but T_{33} , its component in the vorticity direction, is smaller than the temperature in the plane of shear,

$$T_{11} = T_{22} > T_{33}. \quad (4.8)$$

The exact temperature values will depend, in general, on the pair distribution function. In table 1, we present the diagonal terms of the temperature tensor in the dilute limit, obtained from the numerical integration of (4.4) for two different isotropic pair distribution functions, corresponding to a random distribution of hard spheres, $g_{HS}(r) = 1$, and to Batchelor & Green's result for a suspension in a simple shear flow, $g_{BG}(r)$ given by (3.1) (Batchelor & Green 1972*b*). Note that, although, in our numerical simulations, we observe a depletion of permanent doublets in the dilute limit, we first neglect this effect, and compute the temperature terms by numerically calculating the integrals in (4.4) using $g_{BG}(r)$, for all possible angular orientations. As we shall see, for dilute suspensions, this provides a satisfactory approximation to the temperature tensor computed from our numerical simulations. The contribution to the integral of each region in which the mobility functions A and B are divided, i.e.

	$t_{11} = t_{22}$	t_{33}		$t_{11} = t_{22}$	t_{33}
Random hard sphere ($g_{HS}(r)$)	0.3157	0.0811	Simple shear flow ($g_{BG}(r)$)	0.4637	0.1031
Lubrication	0.0040	0.0006	Lubrication	0.0896	0.0117
Intermediate	0.0930	0.0175	Intermediate	0.1531	0.0279
Far-field	0.2187	0.0630	Far-field	0.2210	0.0635

TABLE 1. Temperature tensor in the dilute limit, computed using (4.4)–(4.7) for two different pair distribution functions, one for a hard-sphere distribution, and the other given by Batchelor & Green (1972*b*) for a simple shear flow in the dilute limit, (3.1). Also given is the contribution to the velocity fluctuations coming from the three different regions in which the mobility functions A and B are divided, i.e. the lubrication region ($2 < r \leq 2.01$), the intermediate region ($2.01 < r \leq 2.5$) and the far-field region ($2.5 < r$).

the lubrication, intermediate and far-field regions, is also given in table 1. As expected, the far-field contribution is practically identical in both cases, since, in fact, $g_{BG}(r)$ asymptotically approaches $g_{HS}(r)$ for $r \rightarrow \infty$. On the other hand, the contribution of the lubrication region to the velocity fluctuations is at least an order of magnitude larger if computed using $g_{BG}(r)$ because, in that case, the probability of finding two nearly touching spheres is substantially larger than in the hard-sphere case. Finally, the anisotropy ratio in the dilute limit is similar in both cases, $T_{11}/T_{33} \sim 4$.

4.2. Numerical simulations: simple shear flow and hard sphere distributions

All our simulations were performed using the same values of the interparticle force parameters, i.e. $r_c = 10^{-4}$ and $F_0 = 1$. It appears, however, that the computed values of the suspension temperature are rather insensitive to the particular choice of these parameters, given that our values for the diagonal components of the temperature tensor are similar to those obtained by Yurkovetsky (1996) who for $r_c = 10^{-3}$ performed simulations for a wide range of the interparticle force F_0 ($10^{-4} \leq F_0 \leq 10$) and found only minor changes in the computed suspension temperatures at a given concentration.

In figure 5, we present the diagonal terms of the temperature tensor as a function of the volume fraction, obtained in a simple shear flow by means of Stokesian dynamics simulations. The temperature components T_{11} and T_{22} converge to a common curve in the dilute limit, which is consistent with the existence of an isotropic pair distribution function and indicates that the effect of the particle-depleted region of closed streamlines is not measurable. In addition, the decay of the velocity fluctuations follows the dilute limit scaling given by (4.4), that is, that T_{ij} is proportional to ϕ , even for surprisingly high volume fractions. On the other hand, at larger concentrations, we see that the T_{11} and T_{22} curves separate from each other, which is evidence of the structure developed by the suspension at high concentrations. This is consistent with the fact that, as shown in figure 1, although the pair distribution function has fore–aft symmetry in the dilute limit when the interparticle force is very short-range, i.e. $r_c = 10^{-4}$, this symmetry no longer holds for larger concentrations.

The agreement observed in figure 5, between the suspension temperature computed in the dilute limit using $g_{BG}(r)$ and via the numerical simulations, shows that, as expected, the dominant contribution to the velocity fluctuations arises from two-particle hydrodynamic interactions (see Appendix B for a discussion on the whole velocity autocorrelation function in the dilute limit). We also show in figure 5 that the calculations using $g_{HS}(r) = 1$ provide a surprisingly good estimate for the velocity

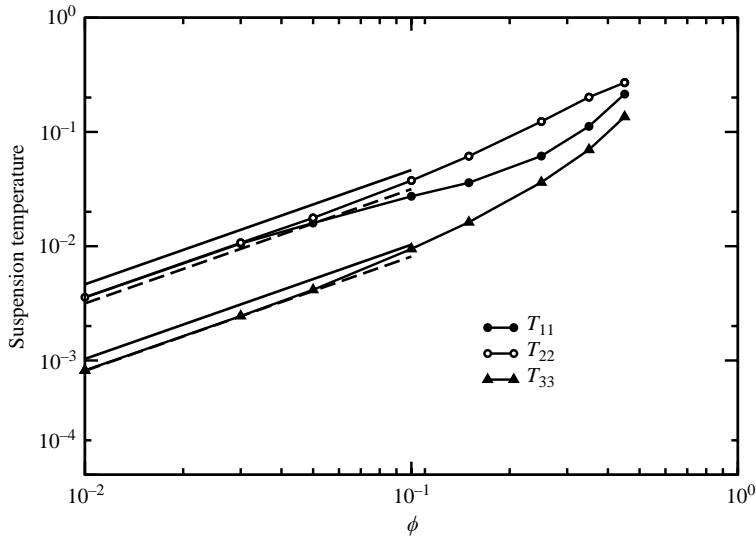


FIGURE 5. Diagonal components of the temperature tensor as a function of the volume fraction, obtained from the numerical Stokesian dynamics simulations. The solid lines correspond to the dilute limit, i.e. two-sphere, calculation using $g_{BG}(r)$ for $T_{ij} = \phi t_{ij}$. The computed values of t_{ij} are given in the second part of table 1 and the discrepancy between the dilute limit theory and the Stokesian dynamics results is about 25% for $\phi < 0.1$. The dashed lines correspond to the dilute limit calculation for $T_{ij} = \phi t_{ij}$, assuming a random distribution of hard spheres, i.e. $g_{HS}(r) = 1$. The computed values of t_{ij} are given in the first part of table 1 and the discrepancy with the Stokesian dynamics results is about 5%, again for $\phi < 0.1$.

fluctuations in sheared suspensions, suggesting that, probably, the effect of the microstructure is not measurable in the dilute limit. This may be because the main difference between the temperatures, as obtained from the two-sphere calculations using either $g_{BG}(r)$ or $g_{HS}(r)$, originates in the contribution of the lubrication region, which is negligible in the $g_{HS}(r) = 1$ case (see table 1). Thus, a lower bound to the velocity fluctuations in the absence of permanent doublets can be estimated roughly using $g_{HS}(r) = 1$. Also, owing to the slow, $O(1/r^2)$, decay of the velocity fluctuations with the distance between spheres, the contribution of the lubrication region to the temperature is relatively minor, $\sim 20\%$, for a pair distribution function given by $g_{BG}(r)$, and should be expected to become even smaller owing to the depletion of permanent doublets. However, the observed excellent agreement between the Stokesian dynamics results for the temperature of sheared suspensions and the temperature obtained from the two-sphere calculations using $g_{HS}(r) = 1$ could not have been expected *a priori* and is a surprising result.

In order to investigate the effects on the temperature of the steady-state microstructure developed by the sheared suspensions, we also performed a second set of numerical computations, in which the velocity fluctuations were calculated for a random hard-sphere distribution of particles subject to simple shear flow. That is, we first generated a random distribution of spheres at the desired concentration. Then, we turned on the simple shear flow at $t = 0$ and computed the instantaneous particle velocities using the Stokesian dynamics code. We then averaged the results over many different realizations of the random hard-sphere distribution. Typically, the number of particles in each realization was the same as in the dynamic simulations, but the number of configurations was increased to $N_c = 256$. We refer to the randomly

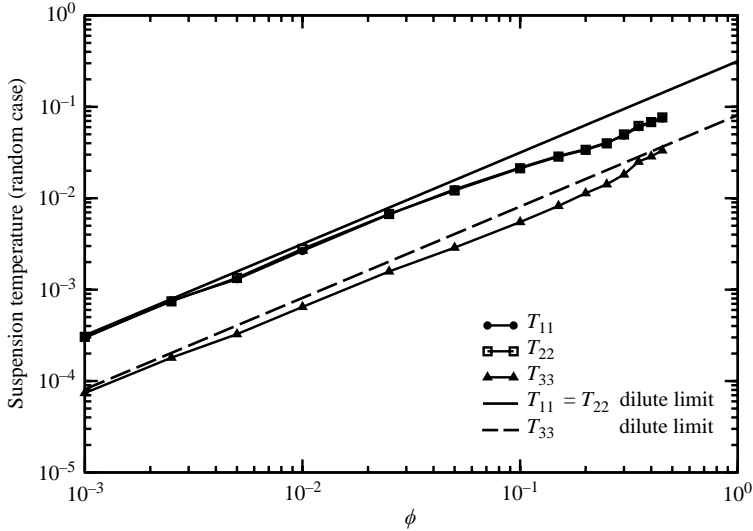


FIGURE 6. Diagonal components of the temperature tensor as a function of the volume fraction, as obtained for a random distribution of hard spheres. We assume that the spheres are subjected to a simple shear flow at time $t = 0$ and compute their instantaneous velocity using the Stokesian dynamics code. The solid and dashed lines correspond to the dilute limit calculation $T_{ij} = \phi t_{ij}$, with t_{ij} given in the first part of table 1.

generated hard-sphere particle distributions as *hard sphere* (HS) distributions in contrast to the *shear flow* (SF) distributions which refer to the particle distributions that are attained asymptotically after the suspension has been sheared in a simple shear flow for strains in excess of 50.

In figure 6, we plot the diagonal components of the temperature tensor, obtained for HS distributions in simple shear flow. We can see that, as a result of the isotropic spatial distribution of particles, T_{11} is equal to T_{22} (within 3%) for all values of the volume fraction. Also, T_{33} , the temperature in the vorticity direction, is smaller than that in the plane of shear, as predicted in the dilute limit. The agreement between the dilute theory and the numerical results at low volume fractions is excellent in this case, with a discrepancy less than 10% at the lowest volume fraction.

As mentioned earlier, the off-diagonal terms of the temperature tensor are expected to be zero for an isotropic pair distribution function. Moreover, if the only broken symmetry in the configurational probability density $P(\mathcal{C}_{\mathcal{N}}|\mathbf{r})$ is the fore-aft symmetry, the only term that may differ from zero is T_{12} , which should actually be negative if particles are depleted in the receding side of the reference sphere, as is observed in the numerical and experimental work. As shown in figure 7, this prediction is borne out by the numerical results, in that, for all volume fractions, all the off-diagonal components vanish for the HS distributions, as well as T_{13} and T_{23} for the SF distributions. Moreover, the remaining off-diagonal component, T_{12} , becomes different from zero only as the concentration increases and a fore-aft asymmetry is developed by the SF distributions, as illustrated by the form of $g_R(\theta)$ shown in figure 1.

4.3. Comparison with experimental results

We now turn to the comparison of the results of our numerical simulations with those found experimentally. Averbakh *et al.* (1997) and Shauly *et al.* (1997) measured T_{11} for concentrations ranging from $\phi = 0.10$ to $\phi = 0.50$. Contrary to our numerical

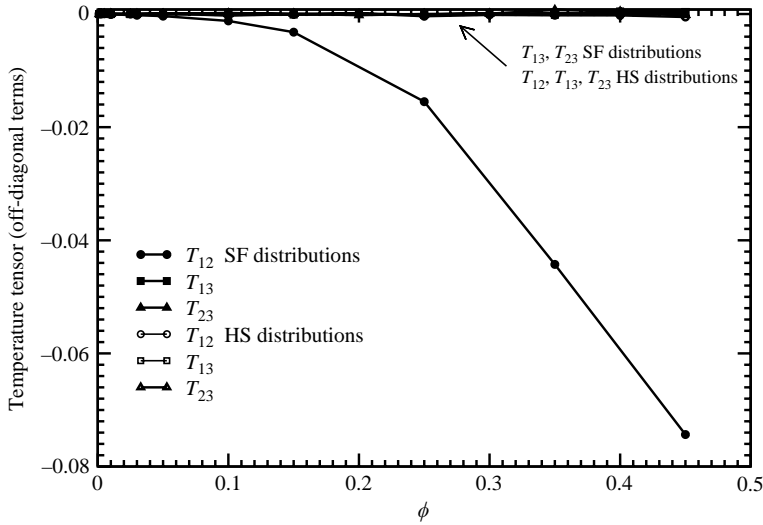


FIGURE 7. Off-diagonal terms of the temperature tensor as a function of the volume fraction.

results, these experimentally measured values of T_{11} showed no dependence on the concentration, probably, as noted by the authors, because the measured fluctuations were dominated by the contribution of the angular rotation of the particles. Although their reported values of T_{11} are of the same order of magnitude as those obtained using Stokesian dynamics simulations for high concentrations, $T_{11} \sim 0.21$ for $\phi \sim 0.45$, they are almost one order of magnitude larger than our values at low concentrations, $T_{11} \sim 0.027$ for $\phi \sim 0.10$.

Lyon & Leal (1998) also measured the fluctuations in the direction of the flow in a two-dimensional channel and found signs that the temperature increased with increasing total concentration. Although the temperatures which they reported seem to be of the same order of magnitude as those we obtained using Stokesian dynamics simulations, quantitative comparisons are subject to considerable uncertainties, because both the local concentration and the local shear rate varied widely across the channels of their experimental set-up.

Shapley *et al.* (2002) examined all the diagonal components of the temperature tensor and reported values for the fluctuations in the direction of shear, $T_{11} \sim 20 - 40$ for $\phi \sim 0.30 - 0.50$, which are not only orders of magnitude larger than those we obtained by means of Stokesian dynamics simulations, $T_{11} \sim 0.27$ for $\phi \sim 0.45$, but, surprisingly, were found to decrease with increasing concentration. Also, in contrast to our results, T_{22} was found to be more than two orders of magnitude smaller than T_{11} . Finally, and in further discrepancy with our results, Shapley *et al.* (2002) found that T_{33} was larger than T_{22} . The reasons for such discrepancies are, at present, unclear.

4.4. Angular velocity fluctuations

A completely analogous analysis to that presented above for the linear velocity fluctuations leads to very similar results for the angular temperature tensor, $\Omega_{ij} = \langle \delta\omega_i \delta\omega_j \rangle$. Specifically, as long as the distribution of spheres has the symmetries discussed previously when the properties of the temperature tensor were analysed, the off-diagonal terms are zero ($\Omega_{ij} = 0, i \neq j$) and $\Omega_{11} = \Omega_{22}$, for all concentrations.

	$\tilde{\Omega}_{11} = \tilde{\Omega}_{22} = \tilde{\Omega}_{33}/5$		$\tilde{\Omega}_{11} = \tilde{\Omega}_{22} = \tilde{\Omega}_{33}/5$
Random hard sphere ($g_{HS}(r)$)	0.01064	Simple shear flow ($g_{BG}(r)$)	0.02260
Lubrication	0.00033	Lubrication	0.00869
Intermediate	0.004438	Intermediate	0.007915
Far-field	0.00587	Far-field	0.00600

TABLE 2. Angular temperature in the dilute limit, computed for two different assumed pair distribution functions, one corresponding to a random distribution of hard spheres, $g_{HS}(r)$, and the other using $g_{BG}(r)$. The contribution to the angular temperature originating from the three different regions in $g_{BG}(r)$ and $C(r)$, cf. (4.13), are noted separately, i.e. the lubrication region ($2 < r \leq 2.01$), the intermediate region ($2.01 < r \leq 2.5$) and the far-field region ($2.5 < r$).

In the dilute limit, the STD of the angular velocity fluctuations can be written as,

$$\Omega_{ij} = \int d\mathbf{r} \delta\omega_i \delta\omega_j (3\phi/4\pi) g(\mathbf{r}) = \phi \left[\frac{3}{4\pi} \int d\mathbf{r} \delta\omega_i \delta\omega_j g(\mathbf{r}) \right] = \phi \tilde{\Omega}_{ij}, \quad (4.9)$$

and for two freely-moving spheres we have (Batchelor & Green 1972a):

$$\delta\omega_1 = -\frac{1}{2} C \frac{x_1 x_3}{r^2}, \quad (4.10)$$

$$\delta\omega_2 = -\frac{1}{2} C \frac{x_2 x_3}{r^2}, \quad (4.11)$$

$$\delta\omega_3 = +\frac{1}{2} C \frac{x_1^2 - x_2^2}{r^2}, \quad (4.12)$$

where C is a dimensionless function of r only. It can then be shown that, for any isotropic pair distribution function, $\Omega_{11} = \Omega_{22} = \Omega_{33}/5$. Finally, using the far-field and the lubrication approximations of $C(r)$ given by Kim & Karrila (1991), and a linear interpolation in the intermediate region,

$$C(r) = \begin{cases} C_l(r) = \frac{-2.283 + 2.3052L + 0.2972L^2}{6.32549 + 6.0425L + L^2} & \text{for } r < 2.01, \\ C_i(r) = \frac{2.5-r}{2.5-2.01} C_l(r) + \frac{r-2.01}{2.5-2.01} C_f(r) & \text{for } 2.01 < r < 2.5, \\ C_f(r) = \frac{5}{2r^3} - \frac{25}{4r^6} + \frac{125}{8r^9} + \frac{25}{r^{10}} + \frac{125}{2r^{11}} & \text{for } 2.5 < r, \end{cases} \quad (4.13)$$

we obtain the results presented in table 2 for $\tilde{\Omega}_{ij}$.

In figures 8 and 9, we present the angular temperature components obtained for the SF and the HS distributions of particles. These temperature components seem to be very sensitive to the microstructure developed by the suspension given that, even at very low concentrations, a difference between Ω_{11} and Ω_{22} can be observed in the SF case, contrary to what happens in the HS case where they coincide for all concentrations, as expected from our previous discussion. Also, the discrepancy between the two-particle dilute limit theory and the numerical values is generally large for the SF distributions (see figure 8 for details), while, in the HS case, there is good agreement with the two-particle dilute limit theory. Not even the linear behaviour on ϕ in the dilute limit seems to have been reached in the SF case at low concentrations, in contrast to what is observed for the HS distributions of spheres, and despite the fact that the perturbations to the angular velocity of a sphere decay even faster than

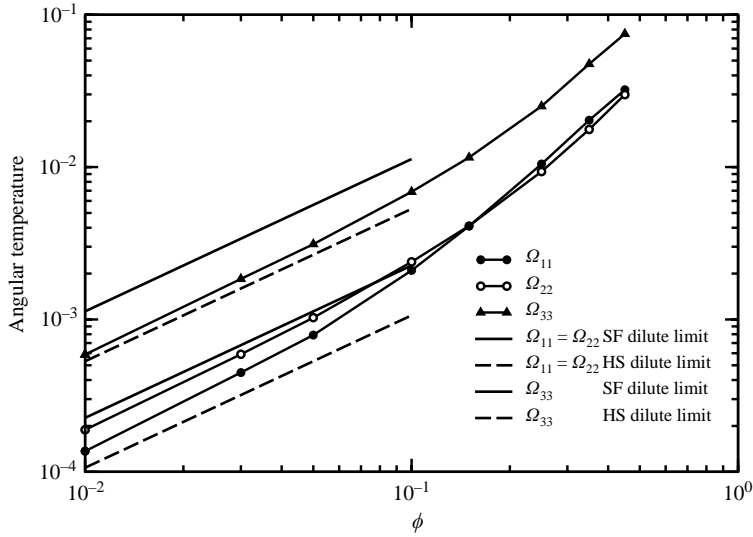


FIGURE 8. Diagonal components of the angular temperature tensor as a function of the volume fraction, obtained from the Stokesian dynamics simulations. The solid and dashed lines correspond to the two-sphere dilute limit calculation for $\Omega_{ij} = \phi \tilde{\Omega}_{ij}$, using $g_{HS}(r)$ (dashed line) and $g_{BG}(r)$ (solid line) pair distribution functions, and the corresponding values of $\tilde{\Omega}_{ij}$ are given in table 2. The ratio between the two-particle theory and the numerical results for the lowest concentration investigated $\phi = 0.01$ is approximately 1.9 for Ω_{33} , 1.2 for Ω_{22} and 1.65 for Ω_{11} .

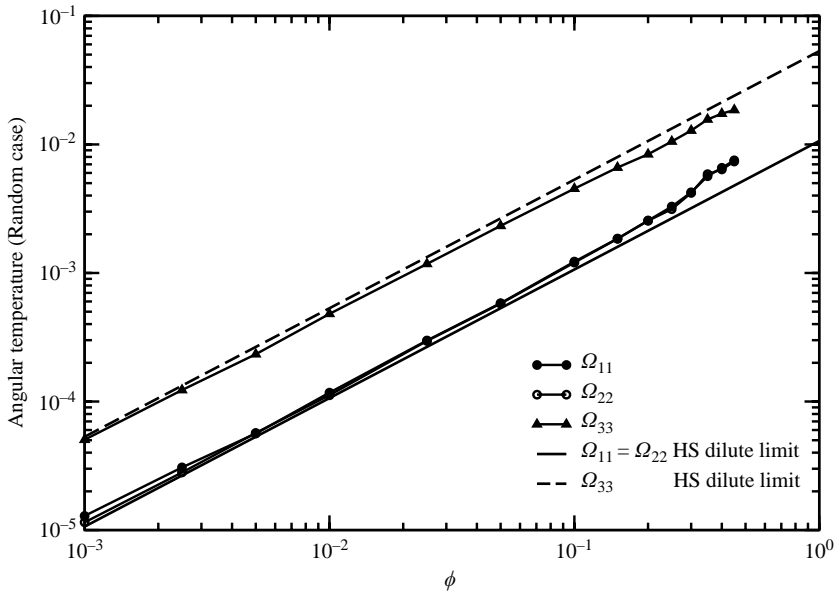


FIGURE 9. Diagonal components of the angular temperature tensor as a function of the volume fraction, obtained for HS distributions. We assume that the spheres are subjected to a simple shear flow at time $t = 0$ and compute their instantaneous angular velocity using the Stokesian dynamics code. The solid and dashed lines correspond to the dilute limit calculation $\Omega_{ij} = \phi \tilde{\Omega}_{ij}$ with $\tilde{\Omega}_{ij}$ being given in the first part of table 2. The difference between the two-particle dilute limit theory and the numerical simulations is less than 20% at the lowest concentrations.

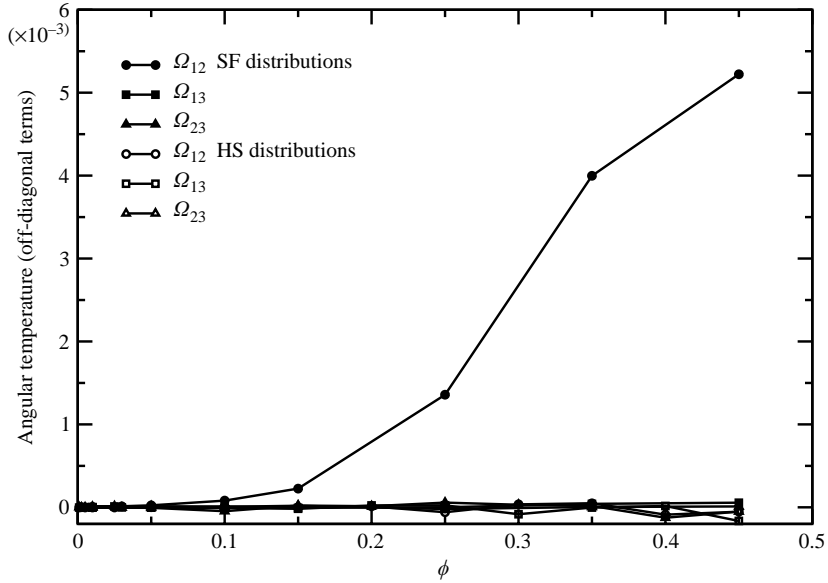


FIGURE 10. Off-diagonal terms of the angular temperature tensor as a function of the volume fraction.

the perturbations to the linear velocity, being $O(1/r^3)$. On the other hand, the faster decay in the interactions with the distance between particles makes the lubrication region more important, now contributing 40% of the total fluctuations, and therefore a more accurate description in this region might be needed to capture the angular temperature. However, we also show in figure 8, that the calculations using $g_{HS}(r)$ provide a lower bound to the angular temperature. Qualitatively, this behaviour may be due to the fact that, as in the case of the linear velocity, the main difference between the angular temperature, as obtained from the two-sphere calculations using either $g_{BG}(r)$ or $g_{HS}(r)$, originates in the contribution of the lubrication region, which is negligible in the $g_{HS}(r) = 1$ case (see table 1). Thus, a lower bound to the angular temperature in the absence of permanent doublets can be estimated roughly using $g_{HS}(r)$.

Finally, we present the off-diagonal terms of the angular temperature tensor (figure 10). As predicted, all terms are negligible in the dilute limit, and only the microstructure developed by the SF distributions leads to a non-zero off-diagonal term Ω_{12} . This is consistent with the result, referred to earlier, that $t_{12} \neq 0$, and with the observed depletion of pairs of particles oriented on the receding side of the interaction (see figure 1).

4.5. Probability density functions of the velocity fluctuations

In addition to the temperature values, the numerical simulations provide us with greater detail about the velocity fluctuations. In fact, we can obtain the full probability distribution function for the fluctuations in both the linear and angular velocity components, calculated from a histogram of the particle velocities, averaged both over N_c different realizations and in time.

In figures 11, 12 and 13, we show the normalized p.d.f. of the linear and angular velocity fluctuations in all directions, and for three different volume fractions. (Note that, for the velocity component in the direction of the shear, we have

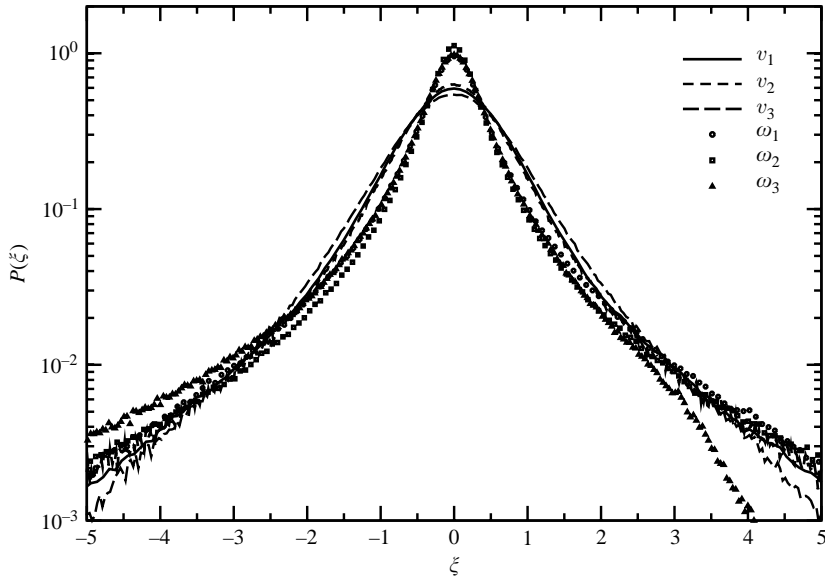


FIGURE 11. Probability density functions for the three components of the linear velocity fluctuations and the three components of the angular velocity fluctuations, at very low concentrations $\phi = 0.01$. All p.d.f.s for the indicated variables, $\delta v_1, v_2, v_3, \omega_1, \omega_2$ and $\delta \omega_3$, are rescaled using the corresponding temperatures so that the standard deviation is unity (for example $\xi = \delta v_1 / \sqrt{T_{11}}$, and similarly for the other variables).

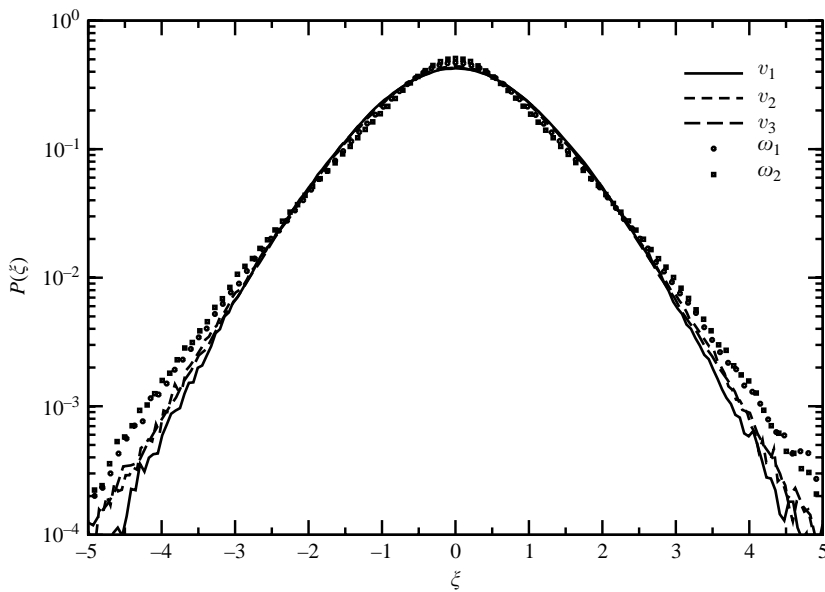


FIGURE 12. Probability density functions for the three components of the linear velocity fluctuations and the two components of the angular velocity fluctuations in the plane of shear. The vorticity component of the angular velocity fluctuations is not symmetric as can be observed in figure 15. The volume fraction is $\phi = 0.10$. All p.d.f.s for the indicated variables, $\delta v_1, v_2, v_3, \omega_1$ and ω_2 , are rescaled using the corresponding temperatures so that the standard deviation is unity (for example $\xi = \delta v_1 / \sqrt{T_{11}}$, and similarly for the other variables).

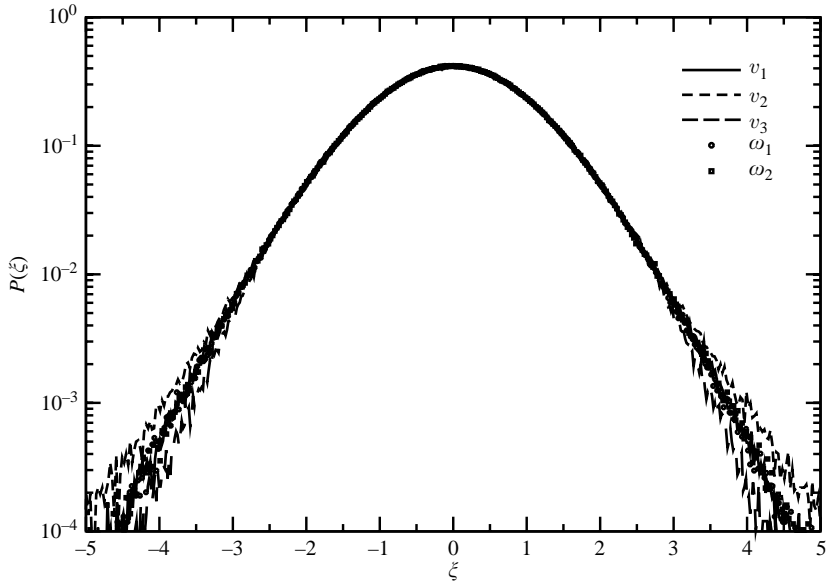


FIGURE 13. Probability density functions for the three components of the linear velocity fluctuations and the two components of the angular velocity fluctuations in the plane of shear. The vorticity component of the angular velocity fluctuations is not symmetric as can be observed in figure 15. The volume fraction is $\phi = 0.45$. All p.d.f.s for the indicated variables, $\delta v_1, v_2, v_3, \omega_1$ and ω_2 , are rescaled using the corresponding temperatures so that the standard deviation is unity (for example $\xi = \delta v_1 / \sqrt{T_{11}}$, and similarly for the other variables).

$P(\xi) \propto \exp(-\beta\xi^\alpha)$														
ϕ	v_i	β	ω_i	β	ϕ	v_i	β	ω_i	β	ϕ	v_i	β	ω_i	β
0.45	v_1	2.54	ω_1	16.1	0.10	v_1	14.1	ω_1	39.2	0.01	v_1	18.1	ω_1	22.8
$\alpha = 2$	v_2	1.85	ω_2	17.8	$\alpha = 1$	v_2	10.9	ω_2	36.0	$\alpha = 1/4$	v_2	18.1	ω_2	21.7
	v_3	4.54				v_3	21.1				v_3	24.8		

TABLE 3. Fitted values for the p.d.f. for the three components of the linear velocity fluctuations and the two components of the angular velocity fluctuations in the plane of shear.

subtracted the contribution of the external velocity field at the centre of the particle, that is $\delta v_1 = \dot{x}_1 - \dot{x}_2$.) Different functional forms are observed as the concentration decreases. A first transition, from Gaussian to exponential distributions occurs when the concentration is decreased from $\phi = 0.45$ to $\phi = 0.10$, as already presented in paper 1. A second transition, from exponential to *stretched* exponential distributions with exponent $\sim 1/4$ occurs when the concentration decreases even further down to $\phi = 0.01$. All the numerical data were fitted using exponential distributions of the form $P(\xi) \propto \exp(-\beta\xi^\alpha)$, with $\alpha = 2$ for large concentrations ($\phi = 0.45$), $\alpha = 1$ for intermediate values of the volume fraction ($\phi = 0.10$), and $\alpha = 1/4$ for very low concentrations ($\phi = 0.01$) with the corresponding values of β given in table 3. In paper 1, we discussed the first transition, from Gaussian to exponential distributions, by analogy with turbulent flows, where this type of transition is observed in the p.d.f. of the velocity differences, the temperature and other passive scalars. The

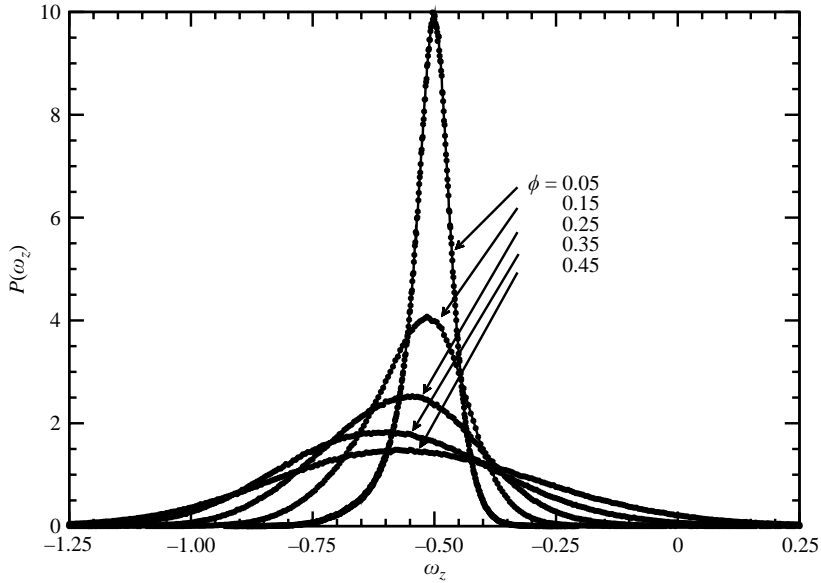


FIGURE 14. Probability density functions of the angular velocity in the vorticity direction, $P(\omega_3)$, for five different volume fractions $\phi = 0.45, 0.35, 0.25, 0.15$ and 0.05 .

second transition presented here is in accordance with that analogy, in that, with decreasing concentrations, the exponent α of the distribution also decreases, implying intermittency, in that the probability of rare events is much larger than expected from Gaussian statistics (Sreenivasan 1999).

Finally, the vorticity component of the angular velocity, ω_3 , has a mean value different from zero, due to the shear flow. In the Stokes limit, by decomposing the linear shear into a purely rotational flow and a purely straining flow, it is easy to show that the angular velocity of a single sphere is $\Omega_3 = -1/2$ (Leal 1992), which is therefore the expected average value of ω_3 in the dilute limit. For larger concentrations, however, hydrodynamic interactions between spheres should be taken into account. However, using the same superposition of flows, and owing to the reflection symmetry of the purely straining flow, it can be shown that the average remains constant, and equal to Ω_3 , even in the presence of other spheres, as long as the distribution of spheres is isotropic. In figure 14, we show the distribution of angular velocities in the vorticity direction, for $\phi = 0.45, 0.35, 0.25, 0.15$ and 0.05 , while in figure 15, we show the mean angular velocity $\langle \omega_3 \rangle$ as a function of the volume fraction. As can be seen, $\langle \omega_3 \rangle$ decreases from $-1/2$ down to -0.58 at $\phi = 0.35$ and then increases to -0.55 at $\phi = 0.45$. (However, note that the shift in $\langle \omega_3 \rangle$ with respect to $\Omega_3 = -1/2$ is always smaller than the width of the distribution, $\sqrt{\Omega_{33}}$, and therefore that the fluctuations are larger than the shift in the average value.) We also show the results obtained for the HS distributions, calculating $\langle \omega_3 \rangle$ using Stokesian dynamics, where it can be seen that the mean angular velocity remains equal to $\Omega_3 = -1/2$ for all concentrations. We can conclude, therefore, that the deviation in the mean angular velocity is due to the anisotropy developed by the suspension in simple shear flows. Moreover, as shown in figure 1, the angular dependence of the pair distribution function for close spheres shows a larger probability for pairs oriented at angles $45^\circ < \theta < 135^\circ$, which is consistent with an increase in the angular speed of the spheres.

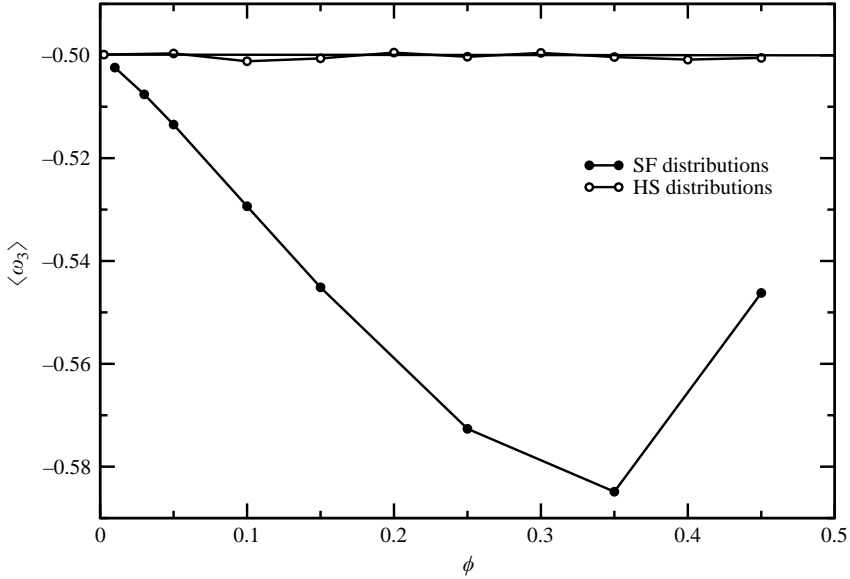


FIGURE 15. Mean value of the angular velocity in the vorticity direction $\langle \omega_3 \rangle$ as a function of the volume fraction ϕ of the suspension. Open symbols corresponds to the same mean angular velocity but for the HS distributions, calculated using the Stokesian dynamics code.

4.6. A note on LDV measurements

It is known that, owing to the random spatial distribution of the scattering sites within the spheres, LDV measurements contain spurious contributions to the linear particle velocity, resulting from the rotation of the particles. Specifically, if the scattering sites are distributed randomly and, on average, uniformly inside the spheres, the STD of the linear velocity fluctuations of such scattering sites in the direction of the flow, T_{11}^{LDV} , can be expressed as,

$$T_{11}^{LDV} = T_{11} + \frac{1}{5}(\Omega_{22} + \Omega_{33} + \langle \omega_3 \rangle^2), \quad (4.14)$$

where T_{11} is the ‘true’ value of the STD of the linear particle velocity fluctuations in the flow direction and the second term on the right-hand side denotes the ‘error’ to the measured STD due to the rotation of the particles. Note that T_{11}^{LDV} refers to the value of T_{11} as would have been extracted from LDV measurements in which the effects of the angular rotation of the spheres are neglected. It is usually assumed that $T_{11}^{LDV} \approx T_{11}$ under most experimental conditions. For example, Lyon & Leal (1998) estimated that the last term in (4.14) was an order of magnitude smaller than T_{11} and therefore neglected its effect, while Shapley *et al.* (2002) explicitly computed this term, and also concluded that its magnitude was negligible compared to T_{11} . In the dilute limit, however, the spurious contributions to T_{11}^{LDV} originating from $\langle \omega_3 \rangle$ are independent of concentration whereas, as shown earlier, the remaining terms on the right-hand side of (4.14) are all proportional to the volume fraction, and their sum equals $T_{11} + (\Omega_{22} + \Omega_{33})/5 = [t_{11} + (\tilde{\Omega}_{22} + \tilde{\Omega}_{33})/5]\phi$ (cf. (4.9)), while $\langle \omega_3 \rangle = \Omega_3 = -1/2$. Therefore, at low concentrations, the mean angular rotation of the spheres dominates the contribution to T_{11}^{LDV} , hence, subtracting $1/20$ is the correction required in this limit. To further illustrate this result we compare, in figure 16, the ‘true’ temperature component T_{11} with: (i) T_{11}^{LDV} , the corresponding temperature as would have been obtained from LDV measurements assuming that the LDV signal is attributed entirely

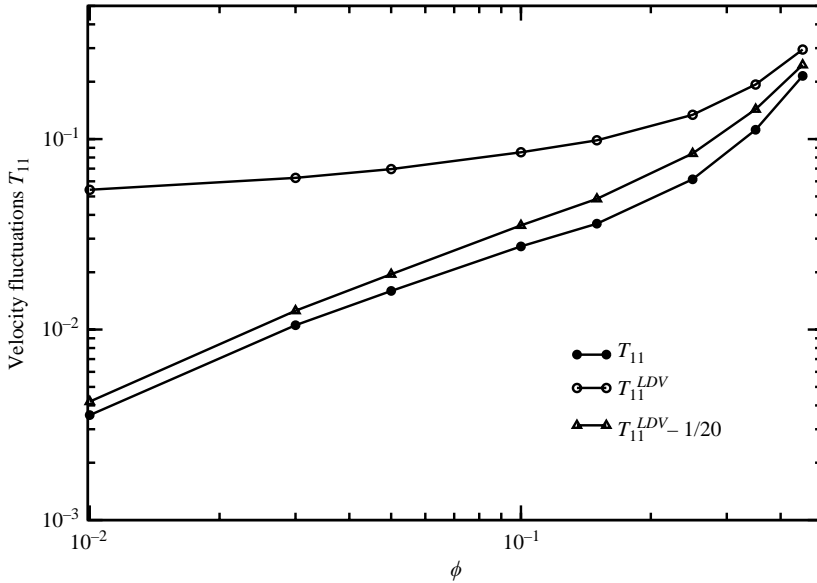


FIGURE 16. Particle velocity fluctuations in the mean flow direction, T_{11} , as computed directly from the numerical simulations (solid circles), as if they had been measured using the LDV technique (open circles) and after correcting these hypothetical LDV measurements to account for the average rotation in the vorticity direction in the dilute limit (open triangles).

to the linear velocity of the particles without accounting for the possible effects of the angular rotation, (cf. (4.14)); and (ii) $T_{11}^{LDV} - 1/20$, the temperature from the same measurements but corrected as suggested above. This simple correction to the analysis of the data remains important even at concentrations as large as 20%, or even larger, and, in fact, the corrected values for T_{11}^{LDV} stay very close to those of the true temperature T_{11} over the whole range of concentrations investigated.

5. Summary

The velocity fluctuations that occur when a simple shear is imposed in a macroscopically homogeneous suspension of neutrally buoyant non-Brownian spheres, and their dependence on the microstructure developed by the suspensions, were investigated in the limit of vanishingly small Reynolds numbers by means of Stokesian dynamics simulations. These simulations account for the hydrodynamic interactions between spheres, and also include a short-range repulsion force that qualitatively models the effects of surface roughness and Brownian forces. We simulated the evolution of a large number of independent initial hard-sphere random distributions for strains $\dot{\gamma}t \sim 100$, which in our previous work, proved sufficiently long to allow us to study the system in the asymptotic fully developed steady state (Drazer *et al.* 2002).

We first discussed the angular structure developed by the suspension undergoing simple shear, and showed that, even for exceedingly short-range interparticle forces, the distribution of particles is fore-aft asymmetric at large concentrations, with a depletion of pairs oriented in the receding side of the reference particle. On the other hand, we showed that the distribution of close particles recovered its expected fore-aft symmetry at low concentrations, but still remained anisotropic, with a depletion of pairs oriented close to the flow direction. We were able to describe accurately the observed anisotropy in the pair distribution function of suspensions

for values of ϕ up to about 5% by integrating $g_{BG}(r)$ only over the region which corresponds to open trajectories and by supposing that permanent doublets were completely absent. We then showed that the pair distribution function obtained by Batchelor & Green (1972*b*) in the dilute limit, $g_{BG}(r)$, accurately follows the simulation results over a wide range of r , including the large increase in the probability of finding pairs of spheres near contact, corresponding to $r \sim 2$, for concentrations up to $\phi \sim 25\%$. However, $g_{BG}(r)$ does not take into account the depletion of permanent doublets, and it is therefore unable to capture the behaviour of the distribution in the limit $r \rightarrow 2$. In fact, in contrast to the divergent behaviour of $g_{BG}(r)$ for $r \rightarrow 2$, the numerical results suggest that $g(r) \sim 0$ for r less than the minimum distance of approach between two spheres in the region of open trajectories ($r_{min} \sim 4 \times 10^{-5}$).

For the velocity fluctuations, we showed that, for an isotropic configurational probability of particles surrounding a reference sphere located at \mathbf{r} , $P(\mathcal{C}_N|\mathbf{r})$, the temperature tensor is diagonal and that the two temperature components in the plane of shear, T_{11} and T_{22} , are equal. Moreover, we showed that, in the dilute limit, all the temperature components are proportional to the volume fraction, and that the temperature components in the plane of shear are larger than that in the vorticity direction. Then, by averaging the velocity fluctuations originated in the hydrodynamic interactions between two spheres, weighted by $g_{BG}(r)$ throughout the whole domain, we computed the temperature tensor in the dilute limit, and found good agreement with the results of our numerical simulations, even for moderately concentrated suspensions. We also showed that the use of a uniform pair distribution function $g_{HS}(r) = 1$ in the dilute limit calculations, provides a surprisingly good approximation to the suspension temperature, suggesting that the effect of the microstructure on the temperature is not measurable. Finally, in Appendix B, we show that the whole velocity autocorrelation function can be predicted, in the dilute limit, using only two-particle encounters.

In contrast, larger discrepancies were found between the corresponding results for the angular temperature and those obtained in the numerical simulations. Even so, in this case, we were able to provide a rough estimate for the lower bound of the angular temperature in the dilute limit, using a uniform pair distribution function $g_{HS}(r) = 1$ in the calculations.

In order to further investigate the effects of the microstructure on the temperature tensor, we performed numerical computations in which we calculated the velocity fluctuations for hard-sphere distributions of particles subject to the same simple shear flow. We also calculated the asymptotic behaviour in the dilute limit, using a uniform pair distribution function $g_{HS}(r) = 1$, and obtained excellent agreement with the numerical results for all the linear and angular velocity fluctuations.

In addition to the temperature tensor, we presented the full probability distribution of the velocity fluctuations for both the linear and the angular velocities, in all directions and for three different volume fractions. We observed different functional forms as the concentration decreases, from a Gaussian to an exponential and finally to a stretched exponential form.

Finally, we presented a simple correction term, involving only the angular velocity of a single sphere in the vorticity direction, which enhances the interpretation of the LDV measurements at intermediate and low volume fractions.

We wish to thank Professor J. F. Brady for the use of his simulation code, for his constructive comments on an earlier version of this paper and for making available to us the PhD thesis of Y. Yurkovetsky. G. D. thanks I. Baryshev for his helpful

comments. This work was partially supported by the Engineering Research Program, Office of Basic Energy Sciences, US Department of Energy under Grants DE-FG02-90ER14139 and DE-FG02-03ER46068; computational facilities were provided by the National Energy Resources Scientific Computer Center.

Appendix A. Expressions for the mobility functions

In this work, we used the expressions for the mobility functions A and B given by da Cunha & Hinch (1996), who divided the interval $r > 2$ into three different regions (see da Cunha & Hinch (1996) for details on how they obtained the expressions for A and B in each region). Specifically: (a) within the *lubrication* region $2 < r \leq 2.01$,

$$A = \frac{(16.3096 - 7.1548r)}{r},$$

$$B = \frac{2(0.4056L^2 + 1.49681L - 1.9108)}{r(L^2 + 6.04250L + 6.32549)},$$

where $L = -\ln(r - 2)$,

(b) within the *intermediate* region $2.01 < r \leq 2.5$,

$$A = -4.3833 + 17.7176\frac{1}{r} + 14.8204\frac{1}{r^2} - 92.4471\frac{1}{r^3} - 46.3151\frac{1}{r^4} + 232.2304\frac{1}{r^5},$$

$$B = -3.1918 + 12.3641\frac{1}{r} + 11.4615\frac{1}{r^2} - 65.2926\frac{1}{r^3} - 36.4909\frac{1}{r^4} + 154.8074\frac{1}{r^5},$$

and (c) within the *far-field* region $r > 2.5$,

$$A = \frac{5}{r^3} - \frac{8}{r^5} + \frac{25}{r^6} - \frac{35}{r^8} + \frac{125}{r^9} - \frac{102}{r^{10}} + \frac{12.5}{r^{11}} + \frac{430}{r^{12}},$$

$$B = \frac{1}{3} \left(\frac{16}{r^5} + \frac{10}{r^8} - \frac{36}{r^{10}} - \frac{25}{r^{11}} - \frac{36}{r^{12}} \right).$$

Appendix B. Velocity autocorrelation function in the dilute limit

In paper 1, we proposed that, in the dilute limit, the whole velocity autocorrelation function converges to an asymptotic function dominated by two-particle encounters. To further investigate this idea we computed the velocity autocorrelation function on the basis of two-particle hydrodynamic interactions only, using (4.5)–(4.7). To this end, we simulated a large number of two-particle encounters ($N_c = 2 \times 10^5$) between a test sphere, initially located at the origin, and an incoming particle, initially far away from the test sphere. The exact position of the incoming particle was chosen randomly in the region $(-\Delta x_1 < x_1^0 < -\Delta x_1 + R, 0 < x_2^0 < R, 0 < x_3^0 < R)$, where R is the size of the cross-section for the incoming particles considered in the calculations. Note that, in order for an encounter to induce a significant velocity fluctuation in the test sphere, both spheres need to come reasonably close to each other at some point during their motion, and we thus used $R = 5$ (Wang, Mauri & Acrivos 1996) (Δx_1 was set to $20R$). The probability distribution used to generate the initial conditions was uniform in x_1 and x_3 , while, in the shear direction we used a probability distribution proportional to the incoming flux of particles in simple shear flow, that is $p(x_2) \propto x_2$. The cross-section of the region of closed streamlines, perpendicular to the flow direction, is so small at $\Delta x_1 = 20R$, that we did not observe any closed trajectory after simulating N_c encounters. The motion of both spheres was then computed, using (4.5)–(4.7) and a time step $\Delta t = 10^{-5}$, until the incoming particle reached the point

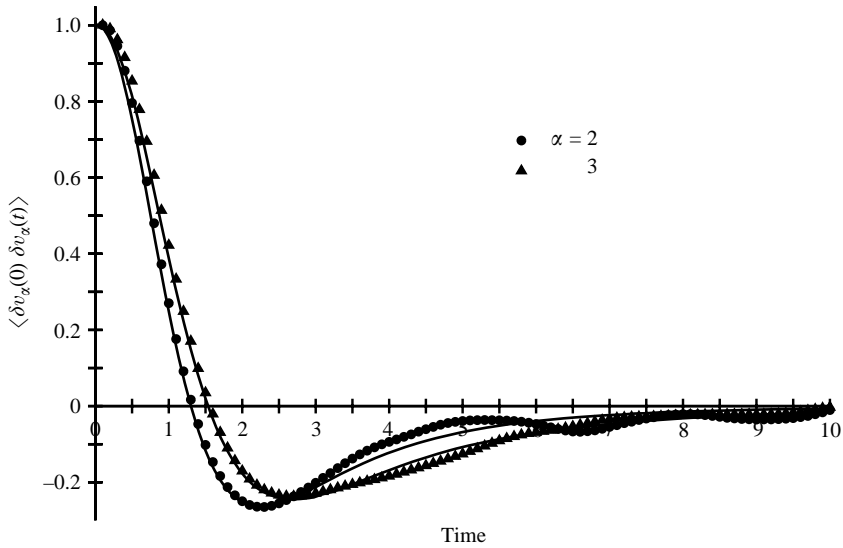


FIGURE 17. Velocity autocorrelation function in the dilute limit in both transverse directions. Symbols correspond to the results obtained using the SD method for a volume fraction $\phi = 0.03$. Solid lines correspond to the numerical computation of the velocity autocorrelation function using two-particle interactions only.

that was symmetric with respect to its initial position, that is $(-x_1^0, x_2^0, x_3^0)$. Finally, the velocity autocorrelation function was computed by averaging over all the simulated trajectories, after splitting each of them into intervals of time $T = 10$. The results are shown in figure 17, where the numerically computed velocity autocorrelation functions in both transverse directions are compared to the results obtained by means of Stokesian dynamics simulations (already presented in paper 1). Excellent agreement is obtained, which confirms that the velocity autocorrelation functions in both transverse directions reach the corresponding asymptotic forms in the dilute limit. It also demonstrates that, as was first suggested in paper 1, the fact that both autocorrelation functions become negative at times $t \sim 1$ is due to the anti-correlated motion performed by the spheres during binary collisions, i.e. the transverse velocities of the spheres involved in a binary collision are reversed at the instant at which the incoming particle goes from the approaching to the receding side of the reference sphere.

REFERENCES

- AVERBAKH, A., SHAULY, A., NIR, A. & SEMIAT, R. 1997 Slow viscous flows of highly concentrated suspensions. I. Laser-doppler velocimetry in rectangular ducts. *Intl J. Multiphase Flow* **23**, 409–424.
- BATCHELOR, G. K. 1972 Sedimentation in a dilute dispersion of spheres. *J. Fluid Mech.* **52**, 245–268.
- BATCHELOR, G. K. & GREEN, J. T. 1972a The hydrodynamic interaction of two small freely-moving spheres in a linear flow field. *J. Fluid Mech.* **56**, 375–400.
- BATCHELOR, G. K. & GREEN, J. T. 1972b The determination of the bulk stress in a suspension of spherical particles to order c^2 . *J. Fluid Mech.* **56**, 401–427.
- BISHOP, J. J., POPEL, A. S., INTAGLIETTA, M. & JOHNSON, P. C. 2002 Effect of aggregation and shear rate on the dispersion of red blood cells flowing in venules. *Am. J. Physiol.-Heart Circul. Physiol.* **283**, H1985–H1996.
- BOSSIS, G. & BRADY, J. F. 1984 Dynamic simulation of sheared suspensions. I. General method. *J. Chem. Phys.* **80**, 5141–5154.

- BRADY, J. F. 2001 Computer simulation of viscous suspensions. *Chem. Engng Sci.* **56**, 2921–2926.
- BRADY, J. F. & BOSSIS, G. 1988 Stokesian dynamics. *Annu. Rev. Fluid Mech.* **20**, 111–140.
- CULLEN, P. J., DUFFY, A. P., O'DONNELL, C. P. & O'CALLAGHAN, D. J. 2000 Process viscometry for the food industry. *Trends Food Sci. Technol.* **11**, 451–457.
- DA CUNHA, F. R. & HINCH, E. J. 1996 Shear-induced dispersion in a dilute suspension of rough spheres. *J. Fluid Mech.* **309**, 211–223.
- DRAZER, G., KOPLIK, J., KHUSID, B. & ACRIVOS, A. 2002 Deterministic and stochastic behaviour of non-Brownian spheres in sheared suspensions. *J. Fluid Mech.* **460**, 307–335.
- GADALA-MARIA, F. & ACRIVOS, A. 1980 Shear-induced structure in a concentrated suspension of solid spheres. *J. Rheol.* **24**, 799–814.
- GOTZ, J., ZICK, K. & KREIBICH, W. 2003 Possible optimisation of pastes and the according apparatus in process engineering by mri flow experiments. *Chem. Engng Process.* **42**, 517–534.
- HUSBAND, D. M. & GADALA-MARIA, F. 1987 Anisotropic particle distribution in dilute suspensions of solid spheres in cylindrical Couette flow. *J. Rheol.* **31**, 95–110.
- VAN KAMPEN, N. G. 1987 *Stochastic Processes in Physics and Chemistry*. North-Holland.
- KIM, S. & KARRILA, S. J. 1991 *Microhydrodynamics: Principles and Selected Applications*. Butterworth–Heinemann.
- KOLLI, V. G., POLLAUFG, E. J. & GADALA-MARIA, F. 2002 Transient normal stress response in a concentrated suspension of spherical particles. *J. Rheol.* **46**, 321–334.
- LEAL, L. G. 1992 *Laminar Flow and Convective Transport Processes*. Butterworth–Heinemann.
- LYON, M. K. & LEAL, L. G. 1998 An experimental study of the motion of concentrated suspensions in two-dimensional channel flow. Part 1. Monodisperse systems. *J. Fluid Mech.* **363**, 25–56.
- MARCHIORO, M. & ACRIVOS, A. 2001 Shear-induced particle diffusivities from numerical simulations. *J. Fluid Mech.* **443**, 101.
- MORRIS, J. F. & KATYAL, B. 2002 Microstructure from simulated brownian suspension flows at large shear rate. *Phys. Fluids* **14**, 1920–1937.
- NOTT, P. R. & BRADY, J. F. 1994 Measurement of shear-induced self-diffusion in concentrated suspensions of spheres. *J. Fluid Mech.* **275**, 157–199.
- PARSI, F. & GADALA-MARIA, F. 1987 Fore-and-aft asymmetry in a concentrated suspension of solid spheres. *J. Rheol.* **31**, 725–732.
- RAMPALL, I., SMART, J. R. & LEIGHTON, D. T. 1997 The influence of surface roughness on the particle-pair distribution function of dilute suspensions of non-colloidal spheres in simple shear flow. *J. Fluid Mech.* **339**, 1–24.
- SHAPLEY, N. C., ARMSTRONG, R. C. & BROWN, R. A. 2002 Laser Doppler velocimetry measurements of particle velocity fluctuations in a concentrated suspension. *J. Rheol.* **46**, 241–272.
- SHAULY, A., AVERBAKH, A., NIR, A. & SEMIAT, R. 1997 Slow viscous flows of highly concentrated suspensions. II. Particle migration, velocity and concentration profiles in rectangular ducts. *Int'l J. Multiph. Flow* **23**, 613–629.
- SIEROU, A. & BRADY, J. F. 2002 Rheology and microstructure in concentrated noncolloidal suspensions. *J. Rheol.* **46**, 1031–1056.
- SREENIVASAN, K. R. 1999 Fluid turbulence. *Rev. Mod. Phys.* **71**, S383–S395.
- VOLTZ, C., NITSCHKE, M., HEYMANN, L. & REHBERG, I. 2002 Thixotropy in macroscopic suspensions of spheres. *Phys. Rev. E* **65**, 051402.
- WANG, Y., MAURI, R. & ACRIVOS, A. 1996 The transverse shear-induced liquid and particle tracer diffusivities of a dilute suspension of spheres undergoing a simple shear flow. *J. Fluid Mech.* **327**, 255–272.
- YURKOVETSKY, Y. 1996 I. Statistical mechanics of bubbly liquids. II. behavior of sheared suspensions of non-Brownian particles. PhD thesis, California Institute of Technology.